Hindawi Publishing Corporation
EURASIP Journal on Advances in Signal Processing
Volume 2008, Article ID 195263, 14 pages
doi:10.1155/2008/195263

Research Article

An Image Content Description Technique for the Inspection of Specular Objects

Y. Caulier[1] and S. Bourennane[2]

[1] *Image Processing and Medical Engineering Department, Fraunhofer Institute, 91058 Erlangen, Germany*
[2] *Multidimensional Signal Group, Fresnel Institute, Ecole Centrale Marseille, 13451 Marseille Cedex 20, France*

Correspondence should be addressed to Y. Caulier, cau@iis.fraunhofer.de

Received 8 May 2008; Accepted 31 July 2008

Recommended by Satya Dharanipragada

This paper proposed an image content description method within the context of specular surface inspection. Such a method is based on a preliminary research concerning the generation of specific stripe patterns for the visual enhancement of defective surface parts of cylindrical specular objects. The goal of this paper is to address the stripe pattern interpretation within a general approach. For this purpose, different pattern recognition processes, consisting not only of the combination of different image segmentation, feature retrieval, and classification, but also of feature combination and selection, will be considered. Three top-down and one bottom-up approaches are evaluated for retrieving the most appropriate feature sets in terms of highest classification rates. It will be demonstrated that following a combination and appropriate selection of these feature sets, even better rates can be reached. With only half of the initial features, an increase of more than 2% is observable.

1. INTRODUCTION

A major challenge of a typical machine vision process is to provide a rugged and cost-effective solution for real-time vision problems. Such an inline vision system ensures identification and rejection of production defects and serves as valuable process feedback and control utilities. A step toward the cost reductions of such processes is to define a general inspection approach that can be applied to a wide range of applications, provided the efforts to adapt such a solution to a specific task are minimal.

Within the field of industrial inspection, the quality control of specular surfaces is most often a manual task. To identify textural or geometrical defects on a specular surface, the human inspector typically has to move the inspected object under appropriate lighting to visually enhance the defective parts. Most industrial machine vision solutions are based on the same principle. They use the deflection of the light rays onto the inspected surfaces to visually enhance the defective parts. Many industrial applications are dedicated to the inspection of metallic car parts [1], large steel plates [2], or steel cylindrical surfaces [3].

In general, specular objects are more difficult to inspect than matt objects. Indeed, in the first case, the camera records the light source *through* the inspected surface, whereas in the second case, the camera observes the light source *on* the inspected surface. As a result, for quality inspections of the surface, conventional inspection techniques defined for matt surfaces such as 3D triangulation are generally not suited for specular surfaces. These must first be covered with a matt film before being inspected, which makes inspection in a real-time environment difficult.

An alternative method to 3D triangulation is provided by deflectometric techniques [4], which are based on the measurement of the reflected light rays projected onto the object of inspection. Different shapes of specular object geometries can be recovered with micrometer resolutions by means of such a technique [5, 6]. However, a preliminary calibration procedure of the recording setup (sensor, lighting) is necessary.

Another possible approach for the inspection of specular surfaces involves adapting the position and the geometry of the projected light rays to visually enhance the defective surface parts so that no 3D reconstruction is necessary

(e.g., a specific lighting arrangement and processing technique for the detection of defects on specular surfaces as proposed by [7, 8]). In a similar manner, [9] determines the orientation of specular surfaces by interpreting the deformations of a known projected light pattern. These applications solely enable the detection of the geometrical deformations of the inspected surface. The detection of other defects is not addressed.

A further possibility is provided by Reindl and O'Leary [10], who uses the light-sectioning technique for the inspection of cylindrical steel probes in an industrial process. In this case, the intensity of the reflected light rays are used to recover the geometry of the surface *and* to determine the periodicity of a surface relief. A technique to reliably retrieve the edges *and* the texture of metallic objects is proposed by [11]. This method is based on the fusion of different images of the same object recorded with varying illumination directions. However, the recording conditions of both approaches are not optimal in terms of a real-time industrial inspection process. The first method implies a complicated movement of the cylindrical objects during their inspection (rotation and translation). With the second method, the whole inspected surface must be recorded several times, which is hardly applicable in an online inspection process.

This paper proposes a general approach for real-time quality control of specular surfaces for industrial surface inspections application. The method is based on the combination of a specific illumination technique and an adapted algorithmic procedure, which was recently proposed for the inspection and characterization purposes of cylindrical specular surfaces [12, 13]. The technique permits the visual *enhancement* and *discrimination* of *various defective parts* of the specular surfaces. The success of an inspection method which uses stripe deformations to discriminate defective from nondefective surfaces depends on the geometry of the stripe pattern depicted in the images. It was demonstrated that it is possible to obtain basic light pattern *periodical and vertical* in case of the inspection of cylindrical shapes [13].

The necessary condition to adapt such an illumination to further object shapes (planar, convex) is that the structured lighting and the recording sensor can be positioned in such a way that a periodical stripe pattern is depicted in the images. It is assumed that such a hardware setup can be defined for further inspection tasks. This paper is therefore dedicated to the generalization of such *periodical and vertical* stripe pattern interpretations.

Various pattern analysis techniques have been proposed since the mid 1960s, that is, since computers were able to solve information handling problems. According to Raudys and Jain [14], the main steps defining a typical pattern recognition process are the following: data collection, pattern classes formation, characteristic features extraction, classification algorithm specification, and estimation of the classification error. The results of each of these steps can be used in a feedback procedure for optimization of the final result. Then, depending on the size and the representativeness of the reference dataset, various classification methodologies can be applied [15].

With the interpretation of such stripe patterns, the task consists in the computation of the most optimal pattern analysis methods in terms of highest classification rates. The core of our approach is dedicated to the *retrieval* and *selection* of the most appropriate feature sets for the characterization of vertical stripe structures.

For the purpose of optimizing the retrieval of the most appropriate features for stripe patterns characterization, a three-step method is proposed. Indeed, such hierarchical feature selection procedures are considered to be particulary suited to complex content-based image description tasks we have here, [16, 17]. Furthermore, in order to address the stripe classification task in general, and in accordance to the recommendations of [14], we emphasis not only on the fact that several feature extraction and feature selection methods, but also various classification algorithms and classification methodologies are taken into consideration.

The first step consists in the evaluation of three different top-down and one bottom-up methodologies. The former are defined within the field of textural analysis and consist of a general approach, the latter are specially defined for the characterization of such structures. This paper is therefore a generalization of the bottom-up method described in [18]. The classification of specular surfaces is addressed by means of fewer stripe features as proposed in this manuscript. The second step is dedicated to the combination of the most relevant features by applying appropriate selection methods. The evaluation criteria for each of these steps is the stripe pattern classification rates. Furthermore, in order to find the most appropriate pattern analysis process and to address such a classification task within a general scope, the combination of five different reference image sets with three different classifiers is considered. The last step consists in the selection of the most appropriate features. For generalization purpose, the use of two different feature selection approaches is taken into consideration.

The new contributions of this article are

(i) at first, to address the inspection of specular surfaces within a general scope based on different image sets, classificators, and classification procedures;

(ii) then, the most appropriate textural features for an automatic inspection of specular surfaces by means of the existing structured illumination are searched;

(iii) in a final step, a new set of adapted stripe features is proposed, and combined with existing features defined for the characterization of fringe patterns;

(iv) the detection accuracy is improved by combining and selecting the most appropriate textural, stripe and fringe features by means of two different and complementary selection methods.

This paper is organized into five sections. Section 2 describes the principle of the specular surface inspection methodology for the visual enhancement of defective surface parts. The three textural top-down and the one adapted bottom-up approaches are introduced in Section 3. Section 4 shows the achieved classification rates for each of the five involved image description methods. The used feature

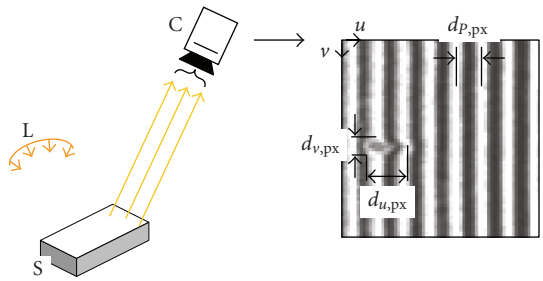

Figure 1: Surface inspection principle for specular objects. The illumination L projects a structured pattern, which is reflected by the inspected surface S and then projected/recorded by a camera C. The generated stripe image depicts a periodical bright and dark stripe structure of period $d_{P,px}$ whose disturbances are synonymous of defective parts. The illumination technique must be defined in such a way that all relevant defects are visually enhanced.

selection methodologies and the corresponding classification rates are addressed in Section 5. Section 6 concludes this paper discussing the classification results.

2. DESCRIPTION OF THE DEFECTIVE SURFACES ENHANCEMENT METHODS

In Section 1, we have seen how a structured light pattern can be adapted for the purpose of specular surface inspection as far as the detection of several defective parts is concerned. An industrial application of such a method is provided as an example [13]. In this case, two types of defects situated on cylindrical metallic objects of approximately 10 mm diameter and up to 2×10^3 mm length must be detected.

The same inspection principle can be adapted to other geometries (planar, convex) of specular objects, where different types of defective parts must be visually enhanced and discriminated. Two conditions are necessary. First, a periodical pattern must be projected onto the imaging sensor. Second, the defective surfaces to discriminate must induce visible deformations of the periodical pattern. Visible means that the deformations synonymous of defective surfaces can be automatically segmented and classified with image processing methods.

Figure 1 shows the inspection principle of a free-form surface based on the method proposed in [13] (the depicted stripe image was recorded with the industrial application).

The figure shows the adapted illumination L whose reflected light rays from the surface S are projected as a periodical stripe pattern onto the recording sensor C. The image resolution in pixel not only along the u- and the v-axis but also along the stripe period $d_{P,px}$ must be chosen according to the minimal size of the defect to detect. Here, a depth defect synonymous of a structural change on the inspected surface of size $d_{u,px}$ and $d_{v,px}$ is depicted.

The pattern recognition process now consists of the automatical characterization and classification of such visually enhanced defects. For the evaluation of the different classification procedures, the images recorded with the industrial application are used. Figure 2 provides an overview of the involved stripe images.

The depicted images were divided into three classes: the acceptable surfaces $\Omega_{A,OK}$, the rejected nonacceptable 2D surfaces $\Omega_{R,2D}$, and the rejected nonacceptable 3D surfaces $\Omega_{R,3D}$. Figure 2(a) shows the three examples of patterns of nondefective surfaces. Figures 2(b) and 2(c) show stripe patterns depicting defective 3D and 2D surfaces. The evaluation criteria for a particular classification procedure was chosen to be the classification rate of such stripe patterns.

3. TEXTURAL AND ADAPTED FEATURE SETS

The main reason for using textural features to characterize stripe structures is to evaluate the classification possibilities offered by such textural algorithms since, to our knowledge, such an elaborate evaluation has never been done before. Textural features were defined to address a broad range of various pattern characterization tasks. The concept of textural analysis is based on the description of local or global image properties. This is closely related to Haralick's concept [19], who defines two basic dimensions: the tonal primitives composing the texture, and their spatial organizations. There is a tremendous number of different pattern characterization approaches which are proposed within the textural analysis community [20]. Thus concerning the interpretation of stripe structures by means of such techniques, a selection of the most appropriate methods is essential.

The selection of representative textural methods for comparisons is partially based on work by Wagner [21], who conducted and presented an extensive comparative study of 18 families of different texture analysis methods from literature, and applied them to seven different reference image datasets in the grey scale domain. The three reference methods selected in this manuscript correlate to the methods described by Wagner with the highest recognition rates from his studies. Moreover, each of these methods is part of the main texture families as considered by [22], namely, the *structural*, the *statistical* and the *transform* approaches. We try to optimize each textural procedure by adapting the innate parameters of each method to the depicted disturbed or nondisturbed stripe pattern, for example, its shape or its intensity.

In terms of stripe structures characterization with *specific* features, most publications are dedicated to identification for classification purposes of fringe patterns depicting bright and dark structures within the field of coherent lighting. A set of six principal fringe structures to characterize and synonymous of defective objects structures is described in [23]. Zhi and Johansson [24] propose a set of 14 geometrical and statistical features for the interpretation of holographical interferometrical fringes for medical purposes. Some features are specifically defined for very particular types of fringe structures, as the "eyes" or the "eyes chains" structures [23], others are defined for the characterization of structures that are similar to the stripe patterns considered in this paper. Further methods involving wavelet [25–27] or Fourier [28] transformations for the characterization of faults have also

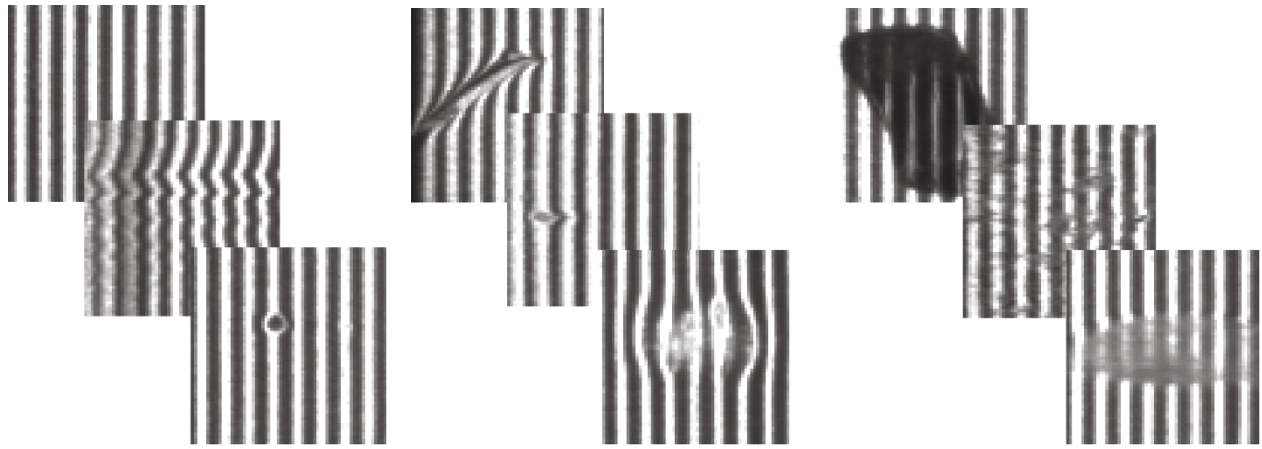

Figure 2: Stripe image examples: (a) three examples of patterns depicting non-defective surfaces, (b) three patterns of defective 3D surfaces and (c) three patterns of defective 2D surfaces. All of the images have a size of $[M_u \times M_v] = [64 \times 64]$ pixels.

been suggested. Such approaches are part of the "transform" methods within the field of textural analysis.

For our purposes, *four geometry-* and *two statistic-based features* proposed by [24] for the characterization of bright stripe patterns are applied. The improvement consists of the completion of these features with further *four specific features* defined within the field of stripe structure characterization. Another novel aspect concerns the use of all of these features not only for the characterization of the bright stripes, but also of the dark stripes in the pattern.

3.1. Textural feature: structural approach

The considered *structural* approach is Chen's [29] method based on statistical and geometrical features of the characterized pattern. The feature computation consists of a two-step procedure. First, the patterns are binarized in the grey level domain by means of several thresholds τ. Then, the connected regions of each binary image are computed. The feature vector $\mathbf{c}^C$ of the pattern is filled with the statistical characteristics of the connected regions of all binarized images. The advantage of using multiple binarizations is to consider different intensity levels of image regions, and to thereby integrate the intensity information in the feature computation.

The stripe patterns present the particularity to have a bimodal grey level distribution corresponding to the distributions of the bright and dark stripe structures. Thus the assumption is made that the consideration of various groups of binarization thresholds τ could lead to an optimization of Chen's feature extraction process. The following four different feature vectors were considered:

$$\begin{aligned}
\mathbf{c}^C_{255}&: \quad N_\mathbf{c} = 16, \quad \tau \in \{0, \ldots, 255\};\\
\mathbf{c}^C_{7}&: \quad N_\mathbf{c} = 16, \quad \tau \in \{32, 64, \ldots, 192, 224\};\\
\mathbf{c}^C_{3}&: \quad N_\mathbf{c} = 16, \quad \tau \in \{64, 128, 192\};\\
\mathbf{c}^C_{1}&: \quad N_\mathbf{c} = 16, \quad \tau \in \{128\};
\end{aligned} \tag{1}$$

Each of these vectors integrates a different number of binarized patterns, however, their lengths all equals 16. In case of vector $\mathbf{c}^C_{255,}$ all possible binarization thresholds τ are used, as only grey level images with a depth of 2^8 are considered.

3.2. Textural feature: statistical approach

The next textural method considered is based on the feature computation as stated by Haralick et al. [30], and is part of the *statistical* texture analysis approach. Such pattern characterization techniques are based on the cooccurrence matrices, a second-order statistical measure of the grey level variation. These matrices indicate the joint probability of the grey level occurrences of all pixel pairs in u- and v-directions in a pattern. Thus optimizing this statistical approach for our purposes consisted of adapting the values of the pixel pair distances d_u and d_v according to the geometry of the stripe structure depicted in the pattern.

The values of d_u were chosen to correspond to the period of the stripe structure, which is a priori known. The values of d_v were chosen to cover the whole range of the disturbance sizes in the v-direction. The following four different feature vectors were considered:

$$\begin{aligned}
\mathbf{c}^H_{1,1}&: \quad N_\mathbf{c} = 14, \quad d_u = 1 \quad d_v = 1;\\
\mathbf{c}^H_{8,1}&: \quad N_\mathbf{c} = 14, \quad d_u = 8 \quad d_v = 1;\\
\mathbf{c}^H_{8,10}&: \quad N_\mathbf{c} = 14, \quad d_u = 8 \quad d_v = 10;\\
\mathbf{c}^H_{8,30}&: \quad N_\mathbf{c} = 14, \quad d_u = 8 \quad d_v = 30.
\end{aligned} \tag{2}$$

Each vector is made up of 14 features as defined by Haralick et al. in [30]. The characterized stripe structures have a period of approximately 8 pixels, so that a value of $d_u = 8$ was repeatedly chosen.

3.3. Textural feature: transform approach

The textural transform approach proposed by Weska [31], and based on the Fourier analysis was used for the characterization of the stripe structures in the spectral domain. The features are computed from amounts of values in the Fourier spectrum corresponding to different spectral regions. Weska [31] defines r_F radial, and d_θ directional frequency regions. His aim is to use the particularity of the spectral domain by selecting various frequency subbands, which is equivalent to retaining certain levels of details and directions in the analyzed patterns. Thus u_F and v_F spectral regions defined along the u-horizontal and the v-vertical image axes were used for the computation of the feature vectors based on the Fourier analysis.

The characterized stripes have a vertical and periodical structure. Thus the directional components in the frequency domain may be strongly discriminative in terms of stripe pattern characterizations. In terms of the stripe pattern analysis, feature vectors integrating diverse subbands of the frequency domain were taken into consideration. The following five different feature vectors were used:

$$\begin{aligned}
\mathbf{c}^{\mathrm{F}}_{r,\theta,v,h} = \{\mathbf{c}^{\mathrm{F}}_r; \mathbf{c}^{\mathrm{F}}_\theta; \mathbf{c}^{\mathrm{F}}_v; \mathbf{c}^{\mathrm{F}}_h\}: &\quad N_{\mathbf{c}} = 33;\\
\mathbf{c}^{\mathrm{F}}_r: &\quad N_{\mathbf{c}} = 8;\\
\mathbf{c}^{\mathrm{F}}_\theta: &\quad N_{\mathbf{c}} = 10;\\
\mathbf{c}^{\mathrm{F}}_v: &\quad N_{\mathbf{c}} = 5;\\
\mathbf{c}^{\mathrm{F}}_u: &\quad N_{\mathbf{c}} = 10.
\end{aligned} \tag{3}$$

The length of each feature vector depends on the considered frequency regions. The vector $\mathbf{c}_{\mathrm{F},r\theta vu}$, considers all possible regions has a maximal length of $N_{\mathbf{c}} = 33$.

3.4. Adapted fringe and stripes features

In contrast to top-down methodologies, as with the three studies cited above, some bottom-up approaches dedicated to the characterization of stripe structures are also described in the literature. Specific geometry-based and intensity-based features have been considered for an adapted characterization of the bright and the dark stripe structures depicted in a stripe pattern **F**. The description of such a pattern is a two-step procedure. It first consists of the *segmentation* at subpixel level of the bright and dark stripes structures, and second of the *characterization* of these segmented structures. Each process is characterized by one parameter: the involved segmentation function f, and the image areas **a** covered by local windows w sliding over the whole described pattern.

A good overview of existing subpixel segmentation techniques is provided by Fisher and Naidu [32]. Such methods are based on the estimation of the peaks to be localized. Specific mathematical functions or local grey level interpolations can be considered. In case of stripe structure characterization, the "Blais-and-Rioux" and the "Center-of-Mass" peak detectors were implemented [32, 33]. Both operators are used for the detection at subpixel level of the bright and the dark stripes along the u-axis of the pattern. In order to be comparable, the same operator's size is considered. A size of 5 elements is retained, as this value corresponds to the length of the bright and the dark peaks to be characterized. The notation for these two peak detectors is br5 for the "Blais-and-Rioux" and cm5 for the "Center-of-Mass". Hence two types of segmentation function are considered $f \in \{\mathrm{br5}; \mathrm{cm5}\}$.

A total of 20 stripe features are used for the characterization of the extracted bright and dark regions. 8 of these features are specially developed for the present purposes, in addition, 12 features were described within the context of fringe structure characterization [24] and adapted for our purposes. Each of these 20 stripe features $\mathrm{c}^S_{\mathrm{a}(m)}(m)$, $m \in \{0, \ldots, 19\}$, represents the average result of an operation $\mathrm{O}_{\mathrm{a}(m)}(m)$ applied to a bright or dark stripe element. The computation of $\mathrm{O}_{\mathrm{a}(m)}(m)$ is applied on an image area $\mathrm{a}(m)$, whose magnitude is feature dependent; see Figure 4. Notations and detailed expressions of the 20 operators $\mathrm{O}_{\mathrm{a}(m)}(00)$ to $\mathrm{O}_{\mathrm{a}(m)}(19)$ can be found in Appendix A.

As the minimal possible size of the reference patterns **F** of the involved image sets is about 20 pixels, the following area magnitudes $\mathrm{a}(i)$ is considered for our purposes: $[5^2]$; $[7^2]$; $[9^2]$; $[11^2]$; $[13^2]$; $[15^2]$; $[17^2]$; $[M_u \times M_v]$. The description of the stripe feature vector is as follows:

$$\begin{aligned}
\mathbf{c}^S_{f,\mathbf{a}}: &\quad N_{\mathbf{c}} = 20;\\
&\quad f \in \{f_{\mathrm{br5}}; f_{\mathrm{cm5}}\};\\
&\quad \mathbf{a} = [\mathrm{a}(0), \ldots, \mathrm{a}(m), \ldots, \mathrm{a}(19)];\\
&\quad \mathrm{a}(m) \in \{[5^2]; [7^2]; [9^2]; [11^2] \ldots\\
&\quad \ldots [13^2]; [15^2]; [17^2]; [M_u \times M_v]\}.
\end{aligned} \tag{4}$$

As mentioned above, the computation of the stripe feature vector relies on two segmentation functions f. Then, each of the stripe feature vector 20 elements can be computed by means of 8 different area sizes of $\mathrm{a}(m)$. Hence 2×8^{20} stripe feature vectors can be retrieved according to the definition given in (4).

In order to reduce the number of possible feature stripe vectors, and thus avoid dimensionality-based problems, a preliminary optimization process to retrieve the most adequate area size of $\mathrm{a}(m)$ for each feature $\mathrm{c}^S_{\mathrm{a}(m)}(m)$ is necessary.

Considering the definitions of the 20 operators outlined in Appendix A, we can distinguish between the features whose computation rely on *fixed* and *adapted* image areas $\mathrm{a}(m)$, where m is the feature index. If we take the two intensity operators as an example, we note that their values computed at pixels ${}^{(B)}s^i_c$ or ${}^{(D)}s^i_c$ are independent on the area sizes of $\mathrm{a}(00)$ or $\mathrm{a}(01)$ centered at these pixels. The only condition is that the area sizes are large enough so that both operators can be applied. In case of the intensity operators, these areas must at least cover the central pixels. The same reasoning can be applied to the operators describing the minimum distance, the maximum distance, and the tangent direction. Hence concerning the 8 features computed with fixed image areas, maximal possible magnitudes of $[M_u \times M_v]$ are considered.

As far as the 12 remaining operators whose computation relies on adapted image areas are concerned, the most appropriate size of each area must be defined according to the stripe structures needed to be characterized. Extensive tests have been conducted in this area and are described previously [18]. These investigations show that an optimal set of image areas can be defined. Such an optimal set is noted $\mathbf{a}^1$. In order to validate the tests described in [18], a further "nonoptimal" set $\mathbf{a}^2$ is taken into consideration. In terms of the adapted image areas, the values of set $\mathbf{a}^2$ are defined as the complementary values of $\mathbf{a}^1$. With respect to the fixed image areas, the values of both sets are identical. These sets are provided in Table 1.

4. CLASSIFICATION OF HIGHLY SPECULAR SURFACES

4.1. Classification procedure

As stated in Section 1, the main purpose of our approach consists of the *definition* and the *selection* of the most appropriate feature sets for the characterization of vertical stripe structures as far as the quality control of specular surfaces is concerned.

The feature sets described in Section 3 are evaluated by means of 5 different image sets and 3 different classificators. Hence for each of the four feature sets, 15 different pattern analysis procedures are considered.

4.1.1. Image sets

One important step in a pattern analysis procedure involves the selection of the characterized image region. With unsupervised image segmentation techniques, segmentation errors are virtually unavoidable [34]. Moreover, among the different stripe pattern characterization techniques described in the literature, none of them propose an automatic segmentation procedure for stripe structures. This is in fact a rather complex task, as the depicted defective surfaces are usually not characterized by sharp contours. Extensive tests and research procedures are necessary to solve the segmentation problem of stripe structures.

As a consequence, hand-segmented image regions have proven to be more reliable. In order to overcome the subjective approach of manually fixing the size of each pattern so that only the disturbed stripe structure is depicted, three sets of inspected surfaces are considered. Segmentation of each set has been done by three different persons. Two other sets of reference patterns with fixed sizes of 64^2 pixels and 128^2 pixels were involved.

Thus, image sets Φ^{ad1}, Φ^{ad2}, Φ^{ad3}, Φ^{64^2}, and Φ^{128^2} will be considered. The size of each set is the same, and the same defects are depicted. These five sets differ only from the size of the depicted images region. The stripe patterns were all recorded with the industrial system [13], typical patterns are depicted in Figure 2.

4.1.2. Classificators

One aim is to evaluate the proposed features *and not* a certain classificator. Hence we "restrain" the classification methodology using two classificators: the *Naive Bayes* NB and the *Nearest-Neighbour k*-NN. The two major reasons for using these classifiers are as follows.

First, both methods are based on two classification models. The NB method is a probabilistic learner which makes the assumption that the feature distributions of each class can be described by a normal-distribution. The *k*-NN is an instance-based prediction model [15] (instance in the sense of pattern) which does not try to create "rules", but works directly on the patterns themselves. Second, the NB classifier is often seen as a simple, but powerful approach. Witten and Frank [15] considers that this classificator often outperforms more sophisticated classifiers. Duda even considers that this classifier led to lowest classification errors from all possible classifiers. In terms of the *k*-NN, Cover and Hart [35] and Gutierrez-Osuna [36] show that this method is known to approach the results of the NB classifier in case of a large dataset as we have here.

Hence three classifiers were used our classification purposes: the Naive Bayes NB, the One-Nearest-Neighbour 1-NN, and the Three-Nearest-Neighbour 3-NN.

4.1.3. Classification methodology

One important aspect concerning the selection of an appropriate classification methodology is the *size* and the *representativeness* of the reference data which are used for the evaluation of the whole classification process. The former is particularly important for the model-based classifiers as the statistical NB method is involved. The latter is directly related with the problem of data over-fitting, which occurs when the classificator is trained on a set of samples that are not representative compared to the set of test samples.

Another possible method to such concerns is to split the reference dataset Φ into multiple training and testing subsets. This process is called the *n*-fold cross-validation. A stratification guarantees the representativeness of each class in the training and testing sets by forcing the folds to retain the same distribution as the original data. Such a cross-validation procedure mitigates any bias due to the overfitting of the data, as the training and testing procedures are repeated *n*-times. When the number of folds equals the number of elements of Φ, the procedure is called leaving-one-out approach. The number *n* of folds is here an important variable. Increasing *n* signifies increasing the number of training data and so reducing the bias due to overfitting. But it is also synonymous to a huger discrepancy of correctly classified patterns across folds as the number of testing data decreases. It is also related to higher computational costs as the entire dataset has to be processed *n* times.

Another splitting technique originally proposed by Efron and Tibshirani [37] is the Bootstrap approach. This method uses the resampling of the original dataset for the generation of *b* multiple training and test sets. If the Bootstrap procedure may be the best way for the classification of small

Table 1: Values of the optimal and "nonoptimal" sets $\mathbf{a}^1$ and $\mathbf{a}^2$ for the 20 stripe features. The maximum possible area size is noted $M^2 = [M_u \times M_v]$.

	00	01	02	03	04	05	06	07	08	09
$\mathbf{a}^1$	M^2	M^2	M^2	M^2	M^2	M^2	17^2	17^2	M^2	M^2
$\mathbf{a}^2$	M^2	M^2	M^2	M^2	M^2	M^2	5^2	5^2	M^2	M^2
$\mathbf{a}^1$	17^2	17^2	17^2	17^2	17^2	17^2	5^2	5^2	17^2	17^2
$\mathbf{a}^2$	5^2	5^2	5^2	5^2	5^2	5^2	17^2	17^2	5^2	5^2

datasets, its major drawback is the high-computational costs as far as the classification of the b datasets has to be done. Moreover, it has not been demonstrated that a bootstrap-based approach outperforms leaving-one-out or other cross-validation procedures [38].

The mostly used approach is certainly the 10-fold stratified cross-validation and according to Witten and Frank [15], a ten times sampling is referred to as the right number of folds to get the best estimation error. Extended tests with various datasets and two classificators have been conducted by Kohavi and John [39] to compare the detection accuracy of the bootstrap technique and the n-fold cross-validation approach for different values of n. Kohavi shows that a stratified 10-fold cross-validation is the more appropriate model in terms of classification accuracy.

Thus the *classification methodology* that will be used for our stripe classification purposes is a stratified 10-F method. Each pattern analysis procedure will be evaluated by means of the classification rates C_P, which gives the number of corrected classified patterns after the stratified 10-fold cross validation of the reference datasets.

C_P is the rate in percent of correctly classified defective surfaces belonging to the three classes $\{\Omega_A; \Omega_{R,3D}; \Omega_{R,2D}\}$, mentioned in the introduction.

4.2. Classification results

The results of the stripe patterns classification by means of Chen's, Haralick's, Fourier's, and Stripe's features, as described by (1), (2), (3) and (4) are provided in Table 4, 5, 6, and 7. Each table provides the rates C_P of correctly classified patterns for the five image sets Φ^{ad1}, Φ^{ad2}, Φ^{ad3}, Φ^{64^2}, Φ^{128^2} and the three classifiers NB, 1-NN, and 3-NN.

The best results for each of the five image set for all the three classifiers are highlighted with an *. The best results for each of the five image sets for the 1-NN classifier are depicted in brackets ( ). Then, best results for all the three classifiers and for all the five image sets are provided in bold face.

These results show that the classification rates are hardly dependent on various factors, such as the selected image region to classify or the involved classificator. Nevertheless, it is obvious that the Fourier method with a rate $C_P = 87.9\%$ and the adapted bottom-up approach with a rate $C_P = 88.9\%$ both outperform Chen's and Haralick's approaches. With the involved classificators, the Nearest-Neighbour method leads to high rates than the Bayes method. In general, the 1-NN leads to higher classification rates than the 3-NN classifier.

With the textural transform approach, lower rates are reached in case of adapted sizes of images patterns, the best results concerns the fixed size of pattern of 64^2 pixels. It is the contrary as far as the classification results using the adapted features are concerned. Higher results in case of the classification with the Φ^{ad1} image set are noticeable.

In a next step, we search to improve the reached classification results by combining the Fourier and the adapted stripe features. Different selection procedures are investigated to evaluate if further improvements of the classification rates can be achieved.

5. SELECTION OF BEST FEATURE SUBSETS

5.1. Feature selection approach

The purpose of a feature subset selection (FSS) process is the generation of a feature subset made of the most relevant information in terms of classification accuracy. Primary research concerning FSS has been addressed for decades by the statisticians community, as [40] for the recognition of handwritten characters or [41] in case of the classification of EKG data. More recently, these FSS techniques have been adapted and completed within the data mining research field, which was primary defined to address the processing of a broader range and huger amount of data.

However, diverse all the FSS techniques can be, such techniques always consist of an iterative procedure, the *generation* and *evaluation* of each new subset, which terminates according to a *stopping criterion*. The performances of each FSS method are defined according to a *validation* process [42].

Two *generation* methods are described in the literature: the *filter* and *wrapper* techniques [15, 36, 43, 44]. The former are independent of the classification process and consist of filtering out the irrelevant data using the feature information content. The latter use the machine learning algorithm or classificator that is used for the learning procedure. In both cases, similar feature search strategies can be applied. We distinguish between a forward selection (the process starts with no selected features), a backward elimination (the process starts with the complete subset), or a bidirectional search strategy which combines both methodologies and starts with a random subset of features [45].

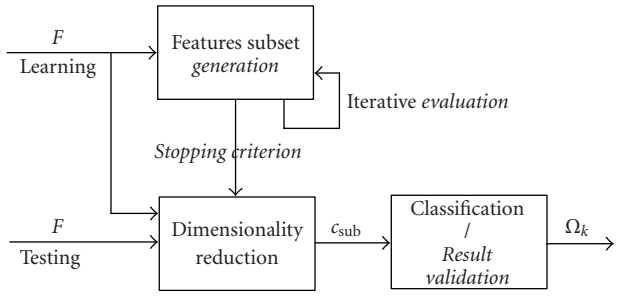

Figure 3: Feature selection principle with the four major parts *generation*, *evaluation*, *stopping criterion*, and *result validation* as described by [42].

The *evaluation* of the generated subset, that is, its goodness, is done according to certain criterion. Reference [42] differentiates two groups: the *independent* criteria typically are used in case of filter models and the *dependent* evaluation criteria are mostly applied as far as wrapper-based FSS models are concerned. The independent criteria are based on the relations between the features eliminating highly correlated characteristics which are redundant for the prediction. Such criteria use the *distances* between the features [46], such as the Bhattacharyya [47] or the Hausdorff distance [48]. The *information gain* [49] or the *dependency* between features [50] are further independent criteria which are used by filter-based feature selection approaches. With the dependent criteria, the evaluation and the optimization of the accuracy rate is done according to the performances of the involved classificator using the selected feature subset. In case of small sets of reference patterns, a cross-validation procedure can often improve the evaluation determination [39].

According to the inspection task, various *stopping criterion* can be addressed. The simplest one is to finish the search of feature subset when all computed features have been selected. The search procedure can also stop when some threshold variables are reached. These can be, for example, the minimum number of features, the maximum number of iterations, or the minimum value of the error rate. More complex procedures as the restriction of the number of backtracking can also determine the stopping conditions. Feature subset search algorithms can also stop when subsequent addition or deletion of any feature does not produce a better subset.

The FSS *validation* is generally done by comparing the classification performances when the full feature is considered and the performances as far as only the computed feature subset are involved.

Figure 3 shows the feature selection principle with the four major parts *generation*, *evaluation*, *stopping criterion,* and *result validation* as described by [42].

The feature selection principle is similar to the pattern classification task, where a learning and a testing phase are considered. The task of selecting the most relevant features is also divided in a training step and a testing step. Once the best feature subset has been computed after a learning phase by means of a reference set of patterns, the validation is done using another set of patterns during the test phase.

5.2. Feature selection results

In order to address the FSS task within the field of stripe pattern characterization, at least one of the two main generation and evaluation families should be involved. Indeed, it is difficult to predict which of the filter or wrapper approaches are more appropriate for our purposes. The latter are often depicted to provide better classification results as the former, as wrapper-based procedures find features better suited to the learning algorithm [36, 44]. However, this should not be considered as a general definition. Hall [43] demonstrated that in small cases, the filter-based correlation-based feature selection (CFS) approach outperforms some wrapper-based approaches. A major drawback of the latter is that such procedures induce high-computational costs, as the whole learning procedure must be invoked at each selection step.

We will therefore consider the CFS filter-based method and the 1-NN wrapper-based approach. The latter was chosen according to the reported classification results of Section 4.2. In order to be comparable, each involved FSS method must be based on the same search procedures and stopping criteria. For both selection processes a feature forward selection procedure with an amount of backtracking of 5 will be addressed. The iterative process starts with an empty initial feature subset. The feature selection *and* the pattern classification follow a 10-F cross-validation procedure. The results are depicted in Table 2.

The results reported in Table 2 show the importance of the reference dataset on the classification accuracy, as far as a combined approach and a selection of the combined two Fourier and stripe feature sets are concerned. In case of image sets whose size is adapted to the characterized surface, the CFS-filter-based approach outperforms the 1-NN-wrapper-based method. Contrariwise, the two image sets with fixed size lead to best classification rates in case of an FSS by means of the wrapper-based method.

So far, we have shown that the directional Fourier and the adapted stripe features are the most appropriate within the context of stripe pattern characterization. We have also seen that the classification accuracy can be increased when appropriate feature selection methods are involved. This means that only a subset of the 30 combined features is really relevant in terms of stripe pattern characterization. Table 3 shows the selected features for the six best classification results involving the 5 datasets and the 2 addressed features selection methods.

The values in Table 3 correspond to the number of times each of the 30 features has been selected after a 10-F cross-validation. The values are comprised between 0 and 10, so that the relevance of each feature is proportional to the value. The 10-time, 9-time, and 8-time selections of a feature are therefore marked with ***, **, and *. We notice that some features have never been selected regardless of the FSS approach or the reference dataset. This is particulary the case for the Fourier directional features. In the same manner, the reported results demonstrate that some features have a

Table 2: Rates C_P of correctly classified patterns for the five image sets Φ^{ad1}, Φ^{ad2}, Φ^{ad3}, Φ^{64^2}, and Φ^{128^2} for the most appropriate Fourier and stripe feature sets as far as a 1-NN classifier is used, see the rates shown by an * in Tables 6 and 7. Classification rates for the five images sets using the combined stripe and Fourier features $\mathbf{c}^{S,F}$. Classification rates after the selection of the most relevant features by means of a filter-based CFS method ${}^{CFS}\mathbf{c}^{S,F}$ and a wrapper-based 1-NN method ${}^{1\text{-NN}}\mathbf{c}^{S,F}$.

	Φ^{ad1}	Φ^{ad2}	Φ^{ad3}	Φ^{64^2}	Φ^{128^2}
$\mathbf{c}^{S}$	(88.9)	(85.6)	(85.8)	(85.9)	(86.2)
$\mathbf{c}^{F}$	(79.2)	(77.4)	(74.7)	(87.9)	(84.4)
$\mathbf{c}^{S,F}$	84.9	84.9	83.7	88.4	84.1
${}^{CFS}\mathbf{c}^{S,F}$	**88.8**	**85.7**	**83.7**	89.6	82.5
${}^{1\text{-NN}}\mathbf{c}^{S,F}$	85.3	84.9	**83.7**	**91.2**	**88.4**

high relevance in terms of stripe pattern characterization. In particular, for the "number of elements" $c^S(18)$ and $c^S(19)$ stripe features and the Fourier directional $c_\theta^F(5)$ and horizontal $c_u^F(4)$ features.

The goodness of a feature selection process can be evaluated not only by means of the reached classification rates, but also in terms of the number of relevant features. This last value can also be retrieved by Table 3. The 1-NN-wrapper-based FSS method applied for the classification of images set Φ^{64^2} leads to a classification rate of 91.2%, which is the highest rate depicted in Table 2. With respect to the selected features using this FSS approach, we observe that nearly half of the 30 initial features have a poor relevance, as these have been selected only 0, 1, or 2 times after the 10-F cross-validation process. Moreover, only six parts of the initial 30 features are highly relevant, as these have been selected at least more than 8 times after the 10-F cross-validation process.

6. CONCLUSION

A general approach of the automatic image-based inspection of specular surfaces has been addressed in this paper. Based on the stripe images generated by an existing illumination technique for the visual enhancement of defective specular surface parts, several pattern recognition processes have been evaluated. The general scope of the stripe image interpretation process as stated in this paper has been addressed by means of the combination of different image segmentation, feature retrieval, pattern classification, feature combination, and feature selection techniques.

It has been showed that best classification rates can be reached in case of a combination of specific top-down and adapted bottom-up feature extraction approaches. It was further demonstrated that higher classification rates could be obtained when appropriate FSS techniques are used. Six parts of the features were highly relevant, whereas only half of them showed to be virtually irrelevant.

Such results are very encouraging, they demonstrate that it was possible to tackle the optimization task of stripe image content description by means of a stepwise and adapted methodology. The optimization process consisted of increasing the stripe pattern detection rates after each step of the pattern recognition process by means of the combination and selection of general and specific approaches.

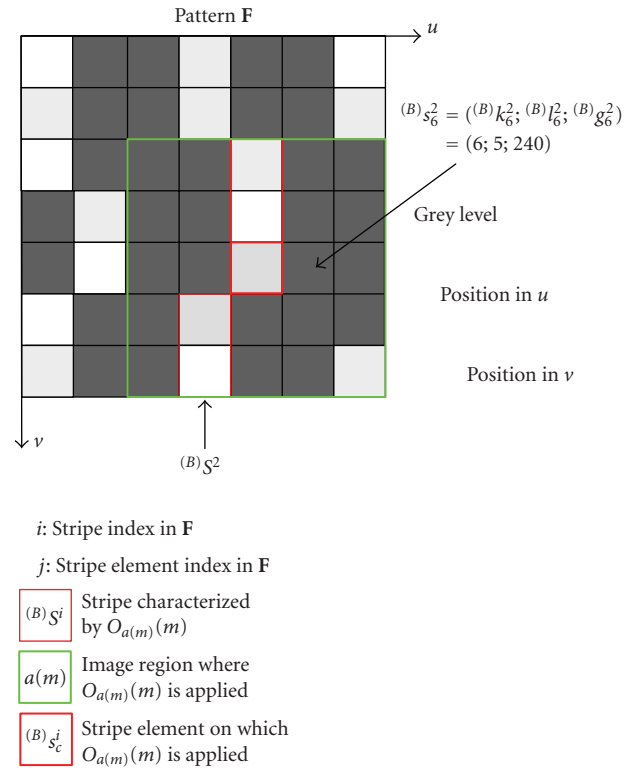

Figure 4: Notation conventions for the computation of the 20 stripe operators.

A similar methodology could be applied in case of the optimization of any processing chain, where each element of the chain interacts with the surrounding elements, and at least influences the output of the chain. The number of possible approaches for each element makes the testing of all the resulting combinations quasi-impossible to realize. Hence stepwise optimization approaches as addressed in this paper are preferred.

APPENDICES

A. EXPRESSIONS OF THE 20 STRIPE OPERATORS

The notations are defined for the bright stripes $^{(B)}$, same notations hold for the dark stripes, in that case $^{(B)}$ should be replaced with $^{(D)}$; see Figure 4.

Table 3: Selected stripe and fourier features for the 6 FSS methods marked in bold face in Table 2. The features are selected using a CFS-based method and a wrapper-1-NN-based method and a 10-F cross-validation. The 10-time, 9-time, and 8-time selected features are marked with ***, **, and *.

	Φ^{ad1}	Φ^{ad2}	Φ^{ad3}	Φ^{ad3}	Φ^{64^2}	Φ^{128^2}
	CFS	CFS	CFS	Wrp	Wrp	Wrp
$c^S(0)$	10***	10***	10***	5	0	0
$c^S(1)$	9**	10***	10***	4	0	0
$c^S(2)$	4	0	0	7	0	1
$c^S(3)$	3	10***	10***	6	2	0
$c^S(4)$	1	9**	9**	0	0	0
$c^S(5)$	0	0	0	5	5	1
$c^S(6)$	6	8*	8*	5	8*	3
$c^S(7)$	4	6	5	8*	6	7
$c^S(8)$	0	0	0	2	5	5
$c^S(9)$	0	0	0	0	8*	7
$c^S(10)$	1	0	0	5	4	1
$c^S(11)$	0	0	0	0	0	0
$c^S(12)$	9**	9**	9**	6	3	4
$c^S(13)$	1	3	3	7	4	5
$c^S(14)$	6	9**	9**	3	3	1
$c^S(15)$	7	0	0	2	1	5
$c^S(16)$	0	0	0	0	1	0
$c^S(17)$	0	0	0	0	0	0
$c^S(18)$	10***	10***	10***	8*	10***	10***
$c^S(19)$	10***	10***	10***	6	8*	7
$c_r^F(0)$	0	0	0	0	—	0
$c_r^F(1)$	1	0	0	2	—	0
$c_r^F(2)$	0	0	2	0	—	0
$c_r^F(3)$	0	0	0	1	—	0
$c_r^F(4)$	0	0	0	3	—	0
$c_r^F(5)$	0	1	2	1	—	0
$c_r^F(6)$	0	0	0	0	—	0
$c_r^F(7)$	0	0	0	0	—	0
$c_\theta^F(0)$	0	0	0	2	0	0
$c_\theta^F(1)$	0	0	0	5	2	7
$c_\theta^F(2)$	0	0	0	1	4	1
$c_\theta^F(3)$	1	0	0	0	4	4
$c_\theta^F(4)$	0	0	0	1	6	8*
$c_\theta^F(5)$	10***	10***	10***	2	10***	6
$c_\theta^F(6)$	0	0	0	1	0	3
$c_\theta^F(7)$	0	0	0	0	1	7
$c_\theta^F(8)$	0	0	0	0	1	5
$c_\theta^F(9)$	0	0	4	2	2	6
$c_v^F(0)$	0	0	0	0	—	0
$c_v^F(1)$	0	0	0	1	—	3
$c_v^F(2)$	0	0	0	0	—	0
$c_v^F(3)$	0	0	0	0	—	0
$c_v^F(4)$	0	0	0	1	—	0
$c_u^F(0)$	0	0	0	0	—	0
$c_u^F(1)$	0	0	0	2	—	0
$c_u^F(2)$	5	0	0	0	—	4
$c_u^F(3)$	0	0	0	0	—	9**

Table 3: Continued.

	Φ^{ad1}	Φ^{ad2}	Φ^{ad3}	Φ^{ad3}	Φ^{64^2}	Φ^{128^2}
	CFS	CFS	CFS	Wrp	Wrp	Wrp
$c_u^{\mathrm{F}}(4)$	10***	10***	9**	1	—	5
$c_u^{\mathrm{F}}(5)$	0	0	0	0	—	0
$c_u^{\mathrm{F}}(6)$	7	0	0	1	—	0
$c_u^{\mathrm{F}}(7)$	0	0	0	0	—	0
$c_u^{\mathrm{F}}(8)$	0	0	0	1	—	0
$c_u^{\mathrm{F}}(9)$	0	0	0	3	—	0

Table 4: Rate C_P of correctly classified patterns for five image sets with Chen's textural features. The best rate C_P for each image set is shown by an *.

	Vector	Φ^{ad1}	Φ^{ad2}	Φ^{ad3}	Φ^{64^2}	Φ^{128^2}
NB	$\mathbf{c}_{255}^{\mathrm{C}}$	74.9	79.5	76.4	77.5	74.8
	$\mathbf{c}_{7}^{\mathrm{C}}$	74.9	77.1	75.7	77.5	74.9
	$\mathbf{c}_{3}^{\mathrm{C}}$	70.9	67.3	66.0	77.3	73.8
	$\mathbf{c}_{1}^{\mathrm{C}}$	57.5	60.4	62.3	77.1	75.9
1-NN	$\mathbf{c}_{255}^{\mathrm{C}}$	81.8	82.4	80.3*	82.4*	75.7*
	$\mathbf{c}_{7}^{\mathrm{C}}$	82.8	80.7	80.4	65.2	72.6
	$\mathbf{c}_{3}^{\mathrm{C}}$	80.1	81.2	80.1	60.8	73.5
	$\mathbf{c}_{1}^{\mathrm{C}}$	75.6	72.6	72.0	57.9	69.8
3-NN	$\mathbf{c}_{255}^{\mathrm{C}}$	82.3*	**83.3***	80.3*	79.4	75.8
	$\mathbf{c}_{7}^{\mathrm{C}}$	80.8	80.8	80.2	78.2	76.6
	$\mathbf{c}_{3}^{\mathrm{C}}$	77.6	75.1	76.2	77.0	76.3
	$\mathbf{c}_{1}^{\mathrm{C}}$	77.4	76.1	77.1	77.2	74.6

$^{(B)}k_s^i$,$^{(B)}k_e^i$: first and last elements positions of $^{(B)}S^i$ in $a(m)$;
$\mathrm{dist1}_{\vec{N}(^{(B)}s_j^i)}$: distance of $^{(B)}s_c^i$ to next bright stripe along $\vec{u}$;
$\mathrm{dist2}_{\vec{N}(^{(B)}s_c^i)}$: distance of $^{(B)}s_c^i$ to next bright stripe along $\vec{u}$;
$\mathrm{length}_{\mathrm{wF}}$: length of a stripe in $a(m)$;
$^{(B)}s_s^i$,$^{(B)}s_e^i$: first and last elements of $^{(B)}S^i$ in $a(m)$;
$^{(B)}\mathrm{dist}_{\mathrm{line}}$: distance of $^{(B)}S^i$ to lines ($^{(B)}s_s^i$;$^{(B)}s_s^i$);
$^{(B)}\#_{a(m)}$: number of elements defining $^{(B)}S^i$ in $a(m)$;
Intensity (grey level) of $^{(B)}s_j^i$, a(m) fixed

$$\mathrm{O}_{a(00)}(00) = {}^{(B)}g_j^i; \tag{A.1}$$

Minimum distance of $^{(B)}S^i$, a(m) fixed

$$\mathrm{O}_{a(02)}(02) = \min\left[\mathrm{dist1}_{\vec{k}(^{(B)}s_j^i)}; \mathrm{dist2}_{\vec{k}(^{(B)}s_j^i)}\right]; \tag{A.2}$$

Maximum distance of $^{(B)}S^i$, a(m) fixed

$$\mathrm{O}_{a(04)}(04) = \max\left[\mathrm{dist1}_{\vec{k}(^{(B)}s_j^i)}; \mathrm{dist2}_{\vec{k}(^{(B)}s_j^i)}\right]; \tag{A.3}$$

Deviation of $^{(B)}S^i$, a(m) variable

$$\mathrm{O}_{a(06)}(06) = \left|\left({}^{(B)}k_e^i - {}^{(B)}k_s^i\right)\right|; \tag{A.4}$$

tangent direction of $^{(B)}S^i$ at $^{(B)}s_j^i$, a(m) fixed

$$\mathrm{O}_{a(08)}(08) = \tan^{-1}\left({}^{(B)}s_j^i\right); \tag{A.5}$$

curvature of $^{(B)}S^i$ at $^{(B)}s_j^i$, a(m) variable

$$\mathrm{O}_{a(10)}(10) = \tan'\left({}^{(B)}s_j^i\right); \tag{A.6}$$

length of $^{(B)}S^i$, a(m) variable

$$\mathrm{O}_{a(12)}(12) = \mathrm{length}_{\ \mathrm{a}(m)}\left({}^{(B)}S^i\right); \tag{A.7}$$

shape of $^{(B)}S^i$, a(m) variable

$$\mathrm{O}_{a(14)}(14) = {}^{(B)}\mathrm{dist}_{\mathrm{line}}/{}^{(B)}\#_{\mathrm{a}(m)}; \tag{A.8}$$

straightness of $^{(B)}S^i$, a(m) variable

$$\mathrm{O}_{a(16)}(16) = \frac{\sum_{j=2}^{(B)n^i}\left|\tan\left({}^{(B)}s_j^i\right) - \tan\left({}^{(B)}s_{j-1}^i\right)\right|}{{}^{(B)}\#_{\mathrm{a}(m)} - 1}; \tag{A.9}$$

number of elements of $^{(B)}S^i$ in a(m), a(m) variable

$$\mathrm{O}_{a(18)}(18) = {}^{(B)}\#_{\mathrm{a}(m)}. \tag{A.10}$$

B. CLASSIFICATION RESULTS

The classification results are shown in Tables 4–7.

Table 5: Rate C_P of correctly classified patterns for five image sets with Haralick's textural features. The best rate C_P for each image set is shown by an *.

	Vector	Φ^{ad1}	Φ^{ad2}	Φ^{ad3}	Φ^{64^2}	Φ^{128^2}
NB	$\mathbf{c}^{\mathrm{H}}_{1,1}$	71.2	69.8	70.2	68.4	55.9
	$\mathbf{c}^{\mathrm{H}}_{8,1}$	69.0	68.5	67.9	58.9	58.7
	$\mathbf{c}^{\mathrm{H}}_{8,10}$	68.1	62.3	61.9	58.0	54.6
	$\mathbf{c}^{\mathrm{H}}_{8,30}$	63.5	59.2	59.8	57.9	52.3
1-NN	$\mathbf{c}^{\mathrm{H}}_{1,1}$	77.2	76.2	77.2	71.0	66.3
	$\mathbf{c}^{\mathrm{H}}_{8,1}$	80.9	80.0*	79.3*	79.4	65.1
	$\mathbf{c}^{\mathrm{H}}_{8,10}$	78.7	77.6	75.4	74.1	62.6
	$\mathbf{c}^{\mathrm{H}}_{8,30}$	81.2	77.9	77.5	72.8*	65.6*
3-NN	$\mathbf{c}^{\mathrm{H}}_{1,1}$	77.1	74.2	76.2	71.6	66.2
	$\mathbf{c}^{\mathrm{H}}_{8,1}$	**83.6***	78.6	76.1	75.6	65.9
	$\mathbf{c}^{\mathrm{H}}_{8,10}$	79.9	77.0	73.9	72.6	62.4
	$\mathbf{c}^{\mathrm{H}}_{8,30}$	80.4	78.2	76.3	69.1	63.1

Table 6: Rate C_P of correctly classified patterns for five image sets with Fourier's textural features. The best rates C_P for each image set are shown by an *. The best rates C_P for each image set and for a 1-NN classifier are depicted in brackets.

	Vector	Φ^{ad1}	Φ^{ad2}	Φ^{ad3}	Φ^{64^2}	Φ^{128^2}
NB	$\mathbf{c}^{\mathrm{F}}_{r\theta vu}$	63.4	62.1	57.2	75.4	61.5
	$\mathbf{c}^{\mathrm{F}}_{r}$	58.3	60.0	58.4	67.2	57.8
	$\mathbf{c}^{\mathrm{F}}_{\theta}$	66.4	64.5	64.5	80.4	55.8
	$\mathbf{c}^{\mathrm{F}}_{v}$	49.2	41.0	44.1	79.3	58.8
	$\mathbf{c}^{\mathrm{F}}_{h}$	54.8	53.9	54.8	41.0	36.2
1-NN	$\mathbf{c}^{\mathrm{F}}_{r\theta vu}$	(79.2*)	(77.4)	(74.7)	84.9	(84.4)
	$\mathbf{c}^{\mathrm{F}}_{r}$	72.7	69.1	65.7	69.8	65.7
	$\mathbf{c}^{\mathrm{F}}_{\theta}$	78.2	73.2	72.5	(**87.9***)	83.6*
	$\mathbf{c}^{\mathrm{F}}_{v}$	76.9	72.7	71.6	79.2	75.9
	$\mathbf{c}^{\mathrm{F}}_{h}$	65.0	63.0	63.8	75.6	61.5
3-NN	$\mathbf{c}^{\mathrm{F}}_{r\theta vu}$	76.2	77.9*	76.3*	85.3	81.3
	$\mathbf{c}^{\mathrm{F}}_{r}$	68.6	67.2	66.2	70.6	65.8
	$\mathbf{c}^{\mathrm{F}}_{\theta}$	75.8	70.4	69.5	81.2	82.5
	$\mathbf{c}^{\mathrm{F}}_{v}$	74.3	70.3	72.0	77.8	75.7
	$\mathbf{c}^{\mathrm{F}}_{h}$	63.9	60.0	61.1	75.6	64.7

Table 7: Rate C_P of correctly classified patterns for five image sets with Stripe's features. The best rates C_P for each image set are shown by an *. The best rates C_P for each image set and for a 1-NN classifier are depicted in brackets.

	Vector	Φ^{ad1}	Φ^{ad2}	Φ^{ad3}	Φ^{64^2}	Φ^{128^2}
NB	$\mathbf{c}^{\mathrm{S}}_{\mathbf{a}^1,\mathrm{br5}}$	84.9	85.9	83.6	84.5	78.3
	$\mathbf{c}^{\mathrm{S}}_{\mathbf{a}^1,\mathrm{cm5}}$	83.7	86.1*	85.2	82.8	60.0
	$\mathbf{c}^{\mathrm{S}}_{\mathbf{a}^2,\mathrm{br5}}$	79.6	85.6	84.3	75.8	61.4
	$\mathbf{c}^{\mathrm{S}}_{\mathbf{a}^2,\mathrm{cm5}}$	77.6	85.7	85.0	73.8	57.1
1-NN	$\mathbf{c}^{\mathrm{S}}_{\mathbf{a}^1,\mathrm{br5}}$	88.1	(85.6)	(85.8*)	85.3	(86.2*)
	$\mathbf{c}^{\mathrm{S}}_{\mathbf{a}^1,\mathrm{cm5}}$	(**88.9***)	82.9	83.5	81.6	82.8
	$\mathbf{c}^{\mathrm{S}}_{\mathbf{a}^2,\mathrm{br5}}$	86.1	85.2	84.8	(85.9*)	83.5
	$\mathbf{c}^{\mathrm{S}}_{\mathbf{a}^2,\mathrm{cm5}}$	84.6	84.7	83.6	78.4	78.8
3-NN	$\mathbf{c}^{\mathrm{S}}_{\mathbf{a}^1,\mathrm{br5}}$	86.5	82.7	83.0	84.3	80.5
	$\mathbf{c}^{\mathrm{S}}_{\mathbf{a}^1,\mathrm{cm5}}$	88.9	82.9	83.5	81.6	82.8
	$\mathbf{c}^{\mathrm{S}}_{\mathbf{a}^2,\mathrm{br5}}$	86.1	85.2	84.8	85.9*	83.5
	$\mathbf{c}^{\mathrm{S}}_{\mathbf{a}^2,\mathrm{cm5}}$	84.6	84.7	83.6	78.4	74.8

ACKNOWLEDGMENT

This work was supported by the Bavarian Research Foundation (Bayerische Forschungsstiftung-BFS).

REFERENCES

[1] P. Marino, M. A. Dominguez, and M. Alonso, "Machine-vision based detection for sheet metal industries," in *Proceedings of the 25th Annual Conference of the IEEE Industrial Electronics Society (IECON '99)*, vol. 3, pp. 1330–1335, San Jose, Calif, USA, November-December 1999.

[2] J. Paakkari, *On-line flatness measurement of large steel plates usinf Moire topography*, Ph.D. thesis, University of Oulu, Oulu, Finland, 1998.

[3] F. Pernkopf, "3d surface inspection using coupled hmms," in *Proceedings of the 17th International Conference on Pattern Recognition (ICPR '04)*, vol. 3, pp. 223–226, Cambridge, UK, August 2004.

[4] G. Häulser, "Verfahren und Vorrichtung zur Ermittlung der Form oder der Abbildungseingenschaften von spieglenden oder transparenter Objekten," Patent DE 19944354 A1, 1999.

[5] S. Kammel, *Deflektometrische Untersuchung spiegelnd reflektierender Freiformflächen*, Ph.D. thesis, University of Karlsruhe, Karlsruhe, Germany, 2004.

[6] M. Petz and R. Tutsch, "Optical 3D measurement of reflecting free formed surfaces," Tech. Rep., Institut für Produktionsmesstechnik - iprom, Technische Universität Braunschweig, Braunschweig, Germany, 2002.

[7] G. Delcroix, R. Seulin, B. Lamalle, P. Gorria, and F. Merienne, "Study of the imaging conditions and processing for the aspect control of specular surfaces," *Journal of Electronic Imaging*, vol. 10, no. 1, pp. 196–202, 2001.

[8] R. Seulin, F. Merienne, and P. Gorria, "Machine vision system for specular surface inspection: use of simulation process as a tool for design and optimization," in *Proceedings of the 5th International Conference on Quality Control by Artificial Vision (QCAV '01)*, Le Creusot, France, May 2001.

[9] S. K. Nayar, A. C. Sanderson, L. E. Weiss, and D. A. Simon, "Specular surface inspection using structured highlight and Gaussian images," *IEEE Transactions on Robotics and Automation*, vol. 6, no. 2, pp. 208–218, 1990.

[10] I. Reindl and P. O'Leary, "Instrumentation and measurement method for the inspection of peeled steel rods," in *Proceedings of IEEE Instrumentation and Measurement Technology Conference(IMTC '07)*, pp. 1–6, Warsaw, Poland, May 2007.

[11] F. P. Leon and J. Beyerer, "Active vision and sensor fusion for inspection of metallic surfaces," in *Intelligent Robots and Computer Vision XVI: Algorithms, Techniques, Active Vision, and Materials Handling*, D. P. Casasent, Ed., vol. 3208 of *Proceedings of SPIE*, pp. 394–405, Pittsburgh, Pa, USA, October 1997.

[12] Y. Caulier and K. Spinnler, Ein neues System zur schnellen Prüfung metallischer Oberflächen von Rohren und Stangen, http://www.iis.fraunhofer.de/bf/ops/produkt/hexacam.jsp.

[13] Y. Caulier, K. Spinnler, S. Bourennane, and T. Wittenberg, "New structured illumination technique for the inspection of high reflective surfaces," *EURASIP Journal on Image and Video Processing*, vol. 2008, Article ID 237459, 14 pages, 2008.

[14] S. Raudys and A. Jain, "Small sample size effects in statistical pattern recognition: recommendations for practitioners," *IEEE Transactions on Pattern Analysis and Machine Intelligence*, vol. 13, no. 3, pp. 252–264, 1991.

[15] I. H. Witten and E. Frank, *Data Mining*, Morgan Kaufmann, San Francisco, Calif, USA, 2005.

[16] J. G. Dy, C. E. Brodley, A. Kak, L. S. Broderick, and A. M. Aisen, " Unsupervised feature selection applied to content-based retrieval of lung images," *IEEE Transactions on Pattern Analysis and Machine Intelligence*, vol. 25, no. 3, pp. 373–378, 2003.

[17] H. Peng, F. Long, and C. Ding, "Feature selection based on mutual information criteria of max-dependency, max-relevance, and min-redundancy," *IEEE Transactions on Pattern Analysis and Machine Intelligence*, vol. 27, no. 8, pp. 1226–1238, 2005.

[18] Y. Caulier, K. Spinnler, T. Wittenberg, and S. Bourennane, "Specific features for the analysis of fringe images," *Journal of Optical Engineering*, vol. 47, no. 5, Article ID 057201, 11 pages, 2008.

[19] R. Haralick, "Statistical and structural approaches to texture," *Proceedings of the IEEE*, vol. 67, no. 5, pp. 786–804, 1979.

[20] M. Tuceyran, "Texture analysis," in *Handbook of Pattern Recognition and Computer Vision*, pp. 207–248, World Scientific, River Edge, NJ, USA, 2nd edition, 1998.

[21] T. Wagner, *Automatische Konfiguration von Bildverarbeitungssysteme*, Shaker, Aachen, Germany, 1999.

[22] A. Materka and M. Strzelecki, "Texture analysis methods—a review," Cost b11 report, brussels, Technical University of Lodz, Institute of Electronics, Ul. Stefanowskiego 18, 90-924 Lodz, Poland, 1998.

[23] W. Jüptner, T. Kreis, U. Mieth, and W. Osten, "Application of neural networks and knowledge-based systems for automatic identification of fault-indicating fringe patterns," in *Interferometry '94: Photomechanics*, vol. 2342 of *Proceedings of SPIE*, pp. 16–26, Warsaw, Poland, May 1994.

[24] H. Zhi and R. B. Johansson, "Interpretation and classification of fringe patterns," in *Proceedings 11th International Conference on Pattern Recognition, Image, Speech and Signal Analysis (IAPR '92)*, vol. 3, pp. 105–108, The Hague, The Netherlands, August-Sepember 1992.

[25] S. Krüger, G. Wernicke, W. Osten, D. Kayser, N. Demoli, and H. Gruber, "Fault detection and feature analysis in interferometric fringe patterns by the application of wavelet filters in convolution processors," *Journal of Electronic Imaging*, vol. 10, no. 1, pp. 228–232, 2001.

[26] S. Krüger, G. K. Wernicke, W. Osten, D. Kayser, N. Demoli, and H. Gruber, "Fault detection and feature analysis in interferometric fringe patterns by the application of wavelet filters in convolution processors," in *Machine Vision Applications in Industrial Inspection VIII*, vol. 3966 of *Proceedings of SPIE*, pp. 145–153, San Jose, Calif, USA, January 2000.

[27] X. Li, "Wavelet transform for detection of partial fringe patterns induced by defects in nondestructive testing of holographic interferometry and electronic speckle pattern interferometry," *Journal of Optical Engineering*, vol. 39, no. 10, pp. 2821–2827, 2000.

[28] K. Qian, H. S. Seah, and A. Asundi, "Fault detection by interferometric fringe pattern analysis using windowed Fourier transform," *Measurement Science and Technology*, vol. 15, no. 8, pp. 1582–1587, 2005.

[29] Y. Chen, M. Nixon, and D. Thomas, "Statistical geometrical features for texture classification," *Pattern Recognition*, vol. 28, no. 4, pp. 537–552, 1995.

[30] R. M. Haralick, K. Shanmugam, and I. Dinstein, " Textural features for image classification," *IEEE Transactions on Systems, Man and Cybernetics*, vol. 3, no. 6, pp. 610–621, 1973.

[31] J. Weska, "A survey of threshold selection techniques," *Computer Graphics and Image Processing*, vol. 7, no. 2, pp. 259–265, 1978.

[32] R. B. Fisher and D. Naidu, "A comparison of algorithms for subpixel peak detection," in *Image Technology*, I. T. J. Sanz, Ed., pp. 385–404, Springer, Berlin, Germany, 1996.

[33] M. Asada, I. Ichikawa, and S. Tsuji, "Determining surface orientation by projecting a stripe pattern," *IEEE Transactions on Pattern Analysis and Machine Intelligence*, vol. 10, no. 5, pp. 749–754, 1988.

[34] R. Unnikrishnan, C. Pantofaru, and M. Hebert, "Toward objective evaluation of image segmentation algorithms," *IEEE Transactions on Pattern Analysis and Machine Intelligence*, vol. 29, no. 6, pp. 929–944, 2007.

[35] T. Cover and P. Hart, "Nearest neighbor pattern classification," *IEEE Transactions on Information Theory*, vol. 13, no. 1, pp. 21–27, 1967.

[36] R. Gutierrez-Osuna, "Pattern analysis for machine olfaction: a review," *IEEE Sensors Journal*, vol. 2, no. 3, pp. 189–202, 2002.

[37] B. Efron and R. Tibshirani, *An Introduction to the Bootstrap*, Chapman & Hall, New York, NY, USA, 1993.

[38] S. M. Weiss, "Small Sample Error Rate Estimation for k-NN Classifiers," *IEEE Transactions on Pattern Analysis and Machine Intelligence*, vol. 13, no. 3, pp. 285–289, 1991.

[39] R. Kohavi and G. H. John, "Wrappers for feature subset selection," *Artificial Intelligence*, vol. 97, no. 1-2, pp. 273–324, 2003.

[40] A. Lakshminarasimhan and B. Dasarathy, "A unified approach to feature selection and learning in unsupervised environments," *IEEE Transactions on Computers*, vol. 24, no. 9, pp. 948–952, 1975.

[41] A. Mucciardi and E. Gose, "A comparison of seven techniques for choosing subsets of pattern recognition properties," *IEEE Transactions on Computers*, vol. 20, no. 9, pp. 1023–1031, 1971.

[42] M. Dash and H. Liu, "Feature selection for classification," *Intelligent Data Analysis*, vol. 1, no. 1–4, pp. 131–156, 1997.

[43] M. A. Hall, *Correlation-based feature selection for machine learning*, Ph.D. thesis, University of Waikato, Hamilton, New Zealand, 1999.

[44] G. H. John, R. Kohavi, and K. Pfleger, "Irrelevant features and the subset selection problem," in *Proceedings of the 11th International Conference on Machine Learning (ICML '94)*, pp. 121–129, New Brunswick, NJ, USA, July 1994.

[45] A. Jain and D. Zongker, "Feature selection: evaluation, application, and small sample performance," *IEEE Transactions on Pattern Analysis and Machine Intelligence*, vol. 19, no. 2, pp. 153–158, 1997.

[46] H. Niemann, *Klassifikation von Mustern*, Springer, Berlin, Germany, 2nd edition, 2003.

[47] A. Djouadi, Ö. Snorrason, and F. D. Garber, "The quality of training sample estimates of the bhattacharyya coefficient," *IEEE Transactions on Pattern Analysis and Machine Intelligence*, vol. 12, no. 1, pp. 92–97, 1990.

[48] D. P. Huttenlocher, G. A. Klanderman, and W. R. Rucklidge, "Comparing images using the hausdorff distance," *IEEE Transactions on Pattern Analysis and Machine Intelligence*, vol. 15, no. 9, pp. 850–863, 1993.

[49] X. M. Liu, K. Li, and H. K. Huang, "Feature selection for handwritten chinese characters based on machine learning," in *Proceedings of the 2nd International Conference on Machine Learning and Cybernetics (ICMLC '03)*, pp. 2399–2402, Xi'an, China, November 2003.

[50] L. Talavera, "Dependency-based feature selection for clustering symbolic data," *Intelligent Data Analysis*, vol. 4, no. 1, pp. 19–28, 2000.